Adaptive numerical algorithms to simulate the dynamical Casimir effect in a closed cavity with different boundary conditions

Paula I. Villar[1] and Alejandro Soba[2]

[1]*Departamento de Física* Juan José Giambiagi*, FCEyN UBA and IFIBA CONICET-UBA, Facultad de Ciencias Exactas y Naturales, Ciudad Universitaria, Pabellón I, 1428 Buenos Aires, Argentina*

[2]*CNEA-CONICET centro Atómico Constituyentes, Avenida General Paz 1499, San Martín, Argentina*

(Received 15 November 2016; revised manuscript received 17 May 2017; published 13 July 2017)

We present an alternative numerical approach to compute the number of particles created inside a cavity due to time-dependent boundary conditions. The physical model consists of a rectangular cavity, where a wall always remains still while the other wall of the cavity presents a smooth movement in one direction. The method relies on the setting of the boundary conditions (Dirichlet and Neumann) and the following resolution of the corresponding equations of modes. By a further comparison between the ground state before and after the movement of the cavity wall, we finally compute the number of particles created. To demonstrate the method, we investigate the creation of particle production in vibrating cavities, confirming previously known results in the appropriate limits. Within this approach, the dynamical Casimir effect can be investigated, making it possible to study a variety of scenarios where no analytical results are known. Of special interest is, of course, the realistic case of the electromagnetic field in a three-dimensional cavity, with transverse electric (TE)–mode and transverse magnetic (TM)–mode photon production. Furthermore, with our approach we are able to calculate numerically the particle creation in a tuneable resonant superconducting cavity by the use of the generalized Robin boundary condition. We compare the numerical results with analytical predictions as well as a different numerical approach. Its extension to three dimensions is also straightforward.

DOI: 10.1103/PhysRevE.96.013307

I. INTRODUCTION

One of the most intriguing and fascinating features of quantum field theory resides in the nontrivial nature of its vacuum states. Quantum fluctuations present in the vacuum are responsible for nonclassical effects that can be experimentally detected. The most well known of such phenomena is the Casimir effect. An even more fascinating feature of the quantum vacuum appears when considering dynamical boundaries conditions. The presence of moving boundaries leads to a nonstable vacuum electromagnetic state, resulting in the generation of real photons, which is an amazing demonstration of the existence of quantum vacuum fluctuations of QED, referred to in the literature as the dynamical Casimir effect (DCE) [1–5].

A scenario of particular interest is a so-called vibrating cavity [6], where the distance between two parallel ideal mirrors changes periodically in time. A moving mirror modifies the mode structure of the electromagnetic vacuum. If the mirror velocity, v, is much smaller than the speed of light, c, then the electromagnetic modes adiabatically adapt to the changes and no excitations occur. Otherwise, if the mirror experiences relativistic motion, changes occur nonadiabatically and the field can be excited out of the vacuum, generating real photons.

The quantum theory of relativistic fields with moving boundaries was first explored by Moore in a remarkably original paper on the quantum formulation of linearly polarized light in a one-dimensional moving cavity [7]. The primary result of this investigation was the discovery that moving mirrors in a vacuum create photons. Later, motivated by developments in quantum field theory in curved spacetime, the specialization to a single moving mirror in Minkowski spacetime was carried out by the authors of Refs. [8,9], who again found that nonuniformly accelerating mirrors generate radiation. From a theoretical point of view, it is widely accepted that the most favorable configuration in order to observe the phenomenon is a vibrating cavity, in which it is possible to produce resonant effects between the mechanical and field oscillations. Although the direct measurement of radiation generated by moving mirrors is an important experimental challenge, it has been asserted [10] that photon creation induced by time-dependent boundary conditions has been observed experimentally in superconducting circuits. This experiment consists of a coplanar waveguide terminated by a superconducting quantum interference device (SQUID), upon which a time-dependent magnetic flux is applied. A related experiment involving a Josephson metamaterial embedded in a microwave cavity has been described in Ref. [11]. These experiments stimulated new theoretical research on role of dynamical Casimir physics in quantum information processing, quantum simulations, and engineering of nonclassical states of light and matter [12–16]. There are also ongoing experiments aimed at measuring the photon creation induced by the time-dependent conductivity of a semiconductor slab enclosed by an electromagnetic cavity [17], as well as proposals based on the use of high-frequency resonators to produce the photons and ultracold atoms to detect the created photons via super-radiance [18]. However, despite this successful setup, no optical frequency photons produced by DCE have been seen yet. The main obstacle to its realization in a straightforward way (by displacement of at least one of the cavity boundaries) is a very low ratio of the boundary velocity to the speed of light accessible nowadays in laboratory experiments. Therefore, the only possibility for DCE observation with nonrelativistic velocities is to accumulate the effect under resonance conditions. Fortunately, recently studies involving superconducting circuits showed the existence of parametric resonance in a

superconducting cavity [19–22]. In Ref. [23], the authors studied thoroughly the nonlinear cavity response, turning these superconducting cavities into promising experimental setups for the DCE.

Research in the field has mainly concentrated on one-dimensional models, which are useful for giving an account of the main physical processes participating in the phenomenon. A cavity made of two perfectly parallel reflecting mirrors, one of which oscillates with a mechanical frequency equal to a multiple of the fundamental of the static cavity (while the other one is at rest) is a typical case where this effect takes place [24–29]. As said before, since the maximal velocity of the boundary mirror that could be achieved under laboratory conditions is very small in comparison with the speed of light, parametric resonance becomes relevant (resonance between the mechanical and field oscillations, where a gradual accumulation of the small changes in the quantum state results finally in a significant effect). Thus, many authors have studied vibrating cavities where the boundary wall performs small harmonic oscillations at twice the unperturbed eigenfrequency of the lowest field mode. In most works, this problem has been analytically studied through an expansion of the equations of motion of the field in terms of the small oscillation amplitude to find an approximative solution [multiple scale analysis (MSA)] [30]. This method represents an improvement of a perturbative approach [24–26] and yields solutions at longer times. Depending on the law of motion of the driven wall, some other asymptotical solutions have been found for cases of harmonic motion [8,31]. In all cases, analytical approximations or strategies are necessary due to the complexity of the problem, which involves a great number of degrees of freedom (those of the field involved). The more realistic case of a three-dimensional cavity is studied in Refs. [30–34]. The important difference between one- and higher-dimensional cavities is that the frequency spectrum in one spatial dimension is equidistant while it is in general nonequidistant for more spatial dimensions. An equidistant spectrum yields strong intermode coupling, whereas in the case of a nonequidistant spectrum only a few or even more modes may be coupled, allowing for exponential photon creation in a resonantly vibrating three-dimensional cavity. In all cases, the equations of motion of the field modes of the electromagnetic field inside vibrating cavities of one or higher dimensions are impossible to solve analytically. In all references cited above, the authors make assumptions that simplify the problem in some way and allow analytical estimation of the particle created in particular regimes.

The electromagnetic field inside a dynamical cavity can be decomposed into components corresponding to the electric field parallel or perpendicular to the moving mirror. It is then possible to introduce vector potentials for each polarization, transverse electric (TE) and transverse magnetic (TM) [31]. The equations of motion for TE modes in a dynamical rectangular cavity are equivalent to the equations of motion for a scalar field with Dirichlet boundary conditions [30]. More complicated boundary conditions, so-called generalized Neumann boundary conditions, emerge when studying TM modes [31,32]. In most of the works cited above, only TE polarization is treated.

The calculations involved in determining the physical outcome of particle creation processes, though trivial to state, are often hard or impossible to complete. Usually it is necessary to find the solution of a set of space- or time-dependent field equations, with initial conditions covering a complete basis of functions. Even though one can rely on simplifying approximations, the set of problems for which solutions can be found analytically is considerably limited. In order to get insight into the whole nonlinear problem with intermode coupling, numerical schemes are much required. In Ref. [35], the author has introduced a formalism allowing numerical investigation of the DCE for scalar particles in a one-dimensional cavity. Introducing a particular parametrization for the time evolution of the field modes yields a system of coupled first-order differential equations with Dirichlet boundary conditions. The solutions of this system determine the number of created particles and can be obtained by means of standard numerics. The author employs this formalism to investigate the creation of real particles in resonant and off-resonant cavities and compares numerical results with analytical predictions. The generalization of this method to higher dimensional cavities is said to be straightforward. This makes it possible to study the TE-mode photon creation in a three-dimensional rectangular cavity because it can be related to the production of massive scalar particles in a one-dimensional cavity [36]. However, as stated by the author, more complicated boundary conditions appearing, for example, when studying TM-mode photons cannot be treated within that numerical approach. On the other hand, in Ref. [37], the authors present a Maple package in order to solve the Moore equation (by considering different trajectories of the wall), so as to compute the number of particles created inside a one-dimensional cavity (also Dirichlet boundary conditions and no extension to higher dimensions) based on Refs. [38–42]. No further numerical approaches of the DCE have been reported for Dirichlet and Neunman boundary conditions. Our first approach in studying the particle creation process in the DCE has been done by considering the experimental setup of a superconducting qubit at one end of the cavity [43]. This particular situation included a more complicated boundary condition (compared to that of Dirichlet and Neunman) and could not be computed in the traditional way. This alternative procedure to computing the particle creation can be extended to different time-dependent boundary conditions as in order to study the particle creation in a vibrating cavity fully numerically.

In the present paper, we shall introduce a detailed numerical approach to simulate DCE and compute the number of particles created by taking into account the intermode coupling and holding all degrees of freedom of the problem. We shall consider different type of boundary conditions for simulating different physical situations: Dirichlet, generalized Neumann, and generalized Robin. For each type of boundary condition considered, we shall study the frequency spectrum inside the vibrating cavity as it is close related to the particle creation process. By introducing numerical considerations of the processes involved in each case, we shall show the particle created and compare the results obtain with analytical predictions. We shall see that our approach reproduces known analytical results and helps shed light into regions where analytical approximates do not work. With this formalism at hand, the DCE can be investigated numerically, making it possible to study a variety of scenarios where no analytical

results are known (large amplitude oscillations or arbitrary wall motions). Of special interest is, of course, the realistic case of the electromagnetic field in a three-dimensional cavity, i.e., TE-mode and TM-mode photon creation. Finally, by introducing generalized Robin boundary conditions (see Ref. [44] for previous studies of this type of time-dependent boundary condition), we can obtain a numerical analysis of particle creation in a tuneable superconducting cavity [23]. The paper is organized as follows: In Sec. II, we discuss the boundary conditions for different situations of a field inside a cavity. In Sec. III, we detail all the procedures applied in our numerical approach. In Sec. IV, we describe the cavity spectrum for different boundary conditions and we show how this spectrum is related to the number of particle creation in each case. We shall compare our numerical results with analytical predictions. Furthermore, we show the particle creation in cases where there are no analytical results obtained. Finally, in Sec. V we make our conclusions.

II. BOUNDARY CONDITIONS

First, we consider a rectangular cavity formed by perfectly conducting walls with dimensions L_x, L_y, and L_z. The wall at $x = L_x$ is at rest for $t < 0$ and starts to move at $t = 0$, following a given trajectory $L_x(t) = L_x - \epsilon A \sin(\Omega t)$, where ϵ is a small dimensionless parameter, Ω is an external frequency, and A is the amplitude of the wall's oscillation. In order to consider the electromagnetic field inside the cavity, we introduce the four-vector potential $A_\mu = (\varphi, \vec{A})$, which satisfies the wave equation $\Box \cdot \vec{A} = 0$.

While for the static walls, the boundaries conditions are the usual ones:

$$\vec{E}_\parallel = 0; \quad \vec{B}_\perp = 0. \tag{1}$$

On the moving walls, however, we must be very careful with the boundary conditions. The electromagnetic field inside a dynamical cavity can be decomposed into components corresponding to the electric field parallel or perpendicular to the moving mirror. It is then possible to introduce vector potentials for each polarization, transverse electric (TE) and transverse magnetic (TM). As the mirror moves in the x direction, one can decompose the electromagnetic field in TE and TM modes with respect to the x axis, as explained, for example, in Ref. [32]. By imposing the boundary conditions in the Lorentz frame (the one in which the mirror is at rest), we can write

$$\vec{\mathrm{E}}^{(\mathrm{TE})} = -\partial_t \vec{\mathrm{A}}^{(\mathrm{TE})}, \quad \vec{\mathrm{B}}^{(\mathrm{TE})} = \nabla \times \vec{\mathrm{A}}^{(\mathrm{TE})}; \tag{2}$$

$$\vec{\mathrm{B}}^{(\mathrm{TM})} = \partial_t \vec{\mathrm{A}}^{(\mathrm{TM})}, \quad \vec{\mathrm{E}}^{(\mathrm{TM})} = \nabla \times \vec{\mathrm{A}}^{(\mathrm{TM})}, \tag{3}$$

which means that we use different vector potentials for each polarization. In terms of these potentials, the boundary conditions are relatively simple. Let us denote by S the laboratory frame and by S' the instantaneous moving frame. In S', the TE vector potential satisfies Dirichlet boundary conditions (DBC) $\vec{\mathrm{A}}'^{(\mathrm{TE})}(x' = 0, y', z', t') = 0$. Therefore, on the moving mirror $\vec{\mathrm{A}}^{(\mathrm{TE})}[x = L_x(t), y, z, t] = 0$. Similarly, for the TM vector potential, it is easy to check that $\eta^\mu \partial_\mu \vec{\mathrm{A}}^{(\mathrm{TM})}[x = L_x(t), y, z, t] = [\partial_x + \dot{L_x}(t)\partial_t]\vec{\mathrm{A}}^{(\mathrm{TM})}[x = L_x(t), y, z, t] = 0$, which is a generalized Neumann boundary condition (NBC) with $\eta^\mu = (\dot{L_x}, 1, 0, 0)$. On the static mirror, the boundary conditions are $\vec{\mathrm{A}}^{(\mathrm{TE})}(x = 0, y, z, t) = 0$ and $\partial_x A_z^{(\mathrm{TM})}(x = 0, y, z, t) = \partial_x A_y^{(\mathrm{TM})}(x = 0, y, z, t) = 0$. This is the same for the other directions of the cavity considering static mirrors at $y = 0$, $y = L_y$, $z = 0$, and $z = L_z$. It is easy to note that by properly taking into account the polarization of the different modes we can find the electromagnetic field inside the cavity since the behavior of each TE vector field is related to the problem of a scalar field subjected to DBC, while the TM vector field deals with generalized NBC. As can be seen, both boundary conditions differ in the fact that one is applied on the field and the other one is applied on its spatial derivative.

In order to simulate all possible cases where the DCE can be tested, we can also consider generalized Robin boundary condition (RBC). In this particular situation, we would be considering the experimental setup of a superconducting waveguide ($L_x \gg L_y, L_z$) ending by a SQUID (located at $x = L_x$), as explained in Sec. I. A time-dependent magnetic flux through the SQUID generates a time-dependent boundary condition. In such a case, the field satisfies the wave equation in the cavity, along with the boundary conditions imposed by the SQUID $\alpha_1(t)\partial_x A(L_x, t) + \alpha_2(t)A(L_x, t) + \alpha_3(t)\dot{A}(L_x, t) = 0$, where α_1, α_2, and α_3 are defined by the physical properties of the cavity. For the static wall of the superconducting waveguide ($x = 0$), we can simply consider NBC or DBC.

So far, we have shown that by solving different boundary conditions, we model different physical situations: TE modes (Dirichlet), TM modes (generalized Neumann), and the experimental setup of a SQUID at one end (generalized RBC). In order to know the electromagnetic field inside the cavity, we just have to consider the TE and TM configuration all together. Moreover, by knowing the initial configuration of the field and the one modified by the boundary conditions at a final time, we can estimate the number of particles created in the cavity. In the following, we shall explain this procedure in detail.

The vector potential field operator can be written in terms of the creation $\hat{a}_n^\dagger$ and annihilation $\hat{a}_n$ operators as

$$A(x, t) = \sum_n^\infty [\hat{a}_n \psi_n(x, t) + \hat{a}_n^\dagger \psi_n^*(x, t)]. \tag{4}$$

Here, $\psi_n(x, t)$ are the mode functions of the field and are chosen so as to satisfied the boundary conditions mentioned above. For $t < 0$, $\psi_n(x, t)$ forms a complete orthonormal set of solutions of the wave equation and each field mode is determined by a non-negative integer n. When the mirror is moving, we do not have a complete orthonormal set of solutions. Then, we should expand each mode with respect to an instantaneous basis for $t > 0$ as

$$\psi_n(x, t) = \sum_{k=1}^\infty Q_k^{(n)}(t)\phi_k(x, t), \tag{5}$$

where k is a positive integer and $Q_k^{(n)}(t)$ are canonical variables to be determined. Inserting the expansion of field modes Eq. (5) into the wave equation and integrating over spatial dimensions lead to the equation of motion for the canonical variables,

expressed as

$$\ddot{Q}_m^{(n)} + \omega_m^2(t) Q_m^{(n)} = \sum_s S_{ms}(t, L_x, \dot{L}_x, \ddot{L}_x, \omega_n, Q_m, Q_s, \dot{Q}_s) Q_s^{(n)} + \sum_s T_{ms}(t, L_x, \dot{L}_x, \ddot{L}_x, \omega_n, Q_m, Q_s, \dot{Q}_s) \dot{Q}_s^{(n)}, \quad (6)$$

where the supraindex n refers to the field eigenstate n. We shall have a set of m equations of motions for each mode n of the field considered. As the free electromagnetic field is an operator which can be written as the sum of an infinite number of harmonic oscillators, the number of field modes involved will be settled by the definition of a frequency cutoff Λ, which will size of the numerical problem to be solved. The frequency of the cavity $\omega_m(t)$ is determined in each case by the boundary condition. We shall see in the following that the field mode equation always has the same structure so it is easy to include all cases in the same numerical approach.

III. NUMERICAL METHOD

In this section, we describe the numerical method used for solving the equation of motion of the field modes determined by different boundary conditions. We shall see that all sets of differential equations are very similar, with Dirichlet being the easiest and Robin being the most complicated.

We shall solve the set of coupled differential equations for the canonical variables $Q_k^{(n)}$ and hence obtain information about the behavior of the field modes, by performing a change of variables so as to reach a new system of one order differential equations:

$$\dot{Q}_m = U_m, \qquad \dot{U}_m = -\omega_m^2(t) Q_m + \sum_s S_{ms}(t, \dots) Q_s + \sum_s T_{ms}(t, \dots) \dot{Q}_s, \quad (7)$$

where $S_{ms}(t, \dots)$ and $T_{ms}(t, \dots)$ are the coefficients accompanying Q_s and $\dot{Q}_s$ in Eq. (6). We have dropped the supraindex for simplicity. The structure of the intermode coupling mediated by the coupling matrix $S_{ms}(t, \dots)$ and $T_{ms}(t, \dots)$ matrices depends on the particular kind of boundary conditions. In most cases, we consider a static wall in $x = 0$ and a moving wall in the x direction, defined as $L_x(t) = L_x - A\epsilon \sin(\Omega t)$, where L_x is the distance of two walls in the static situation, Ω is an external frequency, ϵ is a dimensionless parameter which characterizes the small deviation of the wall from the initial static position, and A is the amplitude of the wall's oscillation. In the particular case of generalized Robin boundary conditions, we consider a SQUID located at $x = L_x$.

The initial conditions, specified for each field mode in all cases, are

$$Q_k^{(n)}(0) = \frac{1}{\sqrt{2\omega_n}} \delta_{k,n}; \quad \dot{Q}_k^{(n)}(0) = -i \sqrt{\frac{\omega_n}{2}} \delta_{k,n}; \quad (8)$$

which indicates that the field modes and their derivatives are continuous at $t = 0$, as long as $L_x(t)$ and $\dot{L}_x$ are smooth functions. For a time dependence of the boundary $L_x(t)$ which is not sufficiently smooth (for example, discontinuities in its time derivative), one may expect spurious particle creation. In Appendix A, we present the different set of differential coupled equations obtained in the case of using Dirichlet, Neumann, and generalized Robin boundary conditions.

For each of the set of differential coupled equations and their initial conditions, we have used an integration scheme based on a fourth-order Runge-Kutta-Merson numerical method between $t = 0$ and a maximum time $t_{\max} > 0$. The goal of this family of solvers is to introduce a control in the time-step size for keeping the error of the solution within a prescribed bound, very useful when in a given problem there are abrupt changes in the coefficients involved [45]. The truncation error of the usual fourth Runge-Kutta methods can be made equal to an approximated expression:

$$\sim h^5 f_5(x_i, f_1, f_2, f_3, f_4) + O(h^6), \quad (9)$$

where h refers to the time increment in each evaluation step. The modifications introduced with Merson algorithms with respect to the normal fourth-order Runge-Kutta method consist in the design of a special function of fifth order for Eq. (9) using a linear combination of the four earlier functions. After some algebra, it is easy to arrive at an expression for an estimated error of this step of integration. This error can be prescribed under a certain defined value and consequently the time step must be chosen in order to accomplish this prescription. If under a certain time step the error estimation is greater than the prescription values, the calculus is reinitiated with a minor time step that matches the estimated error and repeated until the total original time step is reached. Using this procedure, the algorithm can be initiated with a relatively high time step and when the variation of the coefficients or the rapidity of the variations of the solutions require fewer time steps, the local time is turned on and the algorithm alone searches for the time step that maintains the error under the prescribed value. By using this algorithm we can perform integrations without time limitations and can explore solutions at any time scale required.

In all cases, the moving wall is at rest at $t = 0$ and then is turned on for times between $0 < t < t_F$, with $t_F < t_{\max}$, where the wall remains static again. For times $t < 0$ and $t > t_F$, the cavity is a static one and we know the set of orthonormal functions. The quantization of the system is straightforward through creation and annihilation operators:

$$Q_n(t < 0) = \frac{1}{\sqrt{2\omega_n}} (\hat{a}_n e^{-i\omega_n t} + \hat{a}_n^\dagger e^{i\omega_n t}), \quad (10)$$

with frequency $\omega_n(t) = 1/L_x \sqrt{(\pi n)^2 + M^2}$, where L_x is the initial length of the cavity and M is a dimensionless mass parameter (in the case of a three-dimensional cavity). For a one-dimensional cavity, $M = 0$. The time-independent annihilation and creation operators $\hat{a}_n, \hat{a}_n^\dagger$ associated with the particle notion for $t \leqslant 0$ are subject to the commutation relations $[\hat{a}_n, \hat{a}_m] = [\hat{a}_n^\dagger, \hat{a}_m^\dagger] = 0$ and $[\hat{a}_n, \hat{a}_m^\dagger] = \delta_{nm}$. The initial vacuum state $|0, t \leqslant 0\rangle$ is defined by

$$a_n^\dagger |0, t \leqslant 0\rangle = 0 \ \ \forall\, n. \quad (11)$$

When the cavity dynamics is switched on at $t = 0$ and the wall follows the prescribed trajectory $L_x(t)$, the field modes

are coupled. Then, the Q_n can be written as

$$Q_n(t \geqslant 0) = \sum_m \frac{1}{\sqrt{2\omega_m}}\left[\hat{a}_m \epsilon_n^m(t) + \hat{a}_m^\dagger \epsilon_n^{*m}(t)\right], \quad (12)$$

with complex functions $\epsilon_n^m(t)$ that satisfy the equation of modes. When the motion ceases and the wall is at rest again for $t > t_F$, $Q_n(t)$ can be expressed again as

$$Q_n(t \geqslant t_F) = \frac{1}{\sqrt{2\omega_n^F}}\left[\hat{\tilde{a}}_n(t_F) e^{-i\omega_n^F(t)} + \hat{\tilde{a}}_n^\dagger(t_F) e^{i\omega_n^F(t)}\right], \quad (13)$$

where the annihilation and creation operators $\hat{\tilde{a}}_n$, $\hat{\tilde{a}}_m^\dagger$, and ω_n^F correspond to the particle notion for $t \geqslant t_F$. The final vacuum state $|0, t \geqslant t_F\rangle$ is defined by

$$\hat{\tilde{a}}_n^\dagger |0, t \geqslant t_F\rangle = 0 \ \ \forall\, n. \quad (14)$$

As expected, the initial-state particle operators $\hat{a}_n$ and $\hat{a}_n^\dagger$ are linked to the final-state operators $\hat{\tilde{a}}_n$ and $\hat{\tilde{a}}_n^\dagger$ by a Bogoliubov transformation $\hat{\tilde{a}}_n = \sum_m [\alpha_{mn}(t_F)\hat{a}_m + \beta_{mn}^*(t_F)\hat{a}_m^\dagger]$. The total number of particles created in a mode n during the motion of the wall is given by the expectation value of the particle number operator $\hat{\tilde{a}}_n^\dagger \hat{\tilde{a}}_n$ associated with the particle motion for $t \geqslant t_F$ with respect to the initial vacuum state:

$$N_n(t_F) = \langle 0, t \leqslant 0 | \hat{\tilde{a}}_n^\dagger \hat{\tilde{a}}_n^\dagger | 0, t \leqslant 0\rangle = \sum_m |\beta_{mn}(t_F)|^2. \quad (15)$$

This is the way the number of particles created has been computed in the literature, analytically (by solving the Bogoliubov transformation [32,36]) and numerically (by implementing a numerical approach to compute $N_n(t)$ as defined above [36]). However, there is also another possibility to achieve similar results. Herein, we propose an alternative procedure. We can assume the unperturbed final state ($t \geqslant t_F$) to be of the form

$$Q_n(t \geqslant t_F) = \frac{1}{\sqrt{2\omega_n^1}}\left[\hat{A}_n(t_F) e^{-i\omega_n^F t} + \hat{B}_n(t_F) e^{i\omega_n^F t}\right]. \quad (16)$$

We can therefore multiply both terms of the equation by $\exp(-i\omega_n^F t)$ and take the mean value in $t_F < t < t_{\max}$. In this way, we are able to numerically evaluate $|B_n|^2$ and the particle number in field mode n as a function of time as $N_n(t) = |B_n(t)|^2/(2\omega_n^F)$. In our numerical approach, we solve the equation of motion for the field modes (for Dirichlet, generalized Neumann, and generalized Robin boundary conditions) and evaluate the number of particles created in each case. In Appendix B, we show the excellent agreement between our numerical scheme, the analytical prediction of Ref. [32] and the numerical approach proposed in Ref. [36].

Our numerical scheme so as to compute the number of particles created in a mode field for each case considered is basically resumed as (i) the definition of the basis of orthonormal functions satisfying the boundary conditions and the frequency spectrum of each cavity; (ii) the resolution of a set of differential coupled equations for the canonical functions Q_n defined by the boundary conditions chosen; and (iii) computation of $B_n(t)$ so as to estimate the number of particles created.

In order to obtain the numerical results presented in the following sections, we proceed in the following way: Two cutoff parameters Λ (for the field modes considered) and Λ_m (for the number of canonical variables considered) are introduced to make the system of differential equations finite and suitable for a numerical treatment. The system of $n \times m$ coupled differential equations is then evolved numerically from $t = 0$ up to a final time t_F and the expectation value of Eq. (15) is calculated for several times in between. By doing so, we interpret t_F as a continuous variable such that Eq. (15) becomes a continuous function of time. Consequently, the stability of the numerical solutions with respect to the cutoffs has to be ensured. In particular, Λ will be chosen such that the numerical results for the number of particles created in single modes are stable. In most cases, it is enough to choose $\Lambda_m = \Lambda$. In our units, the spectral modes $k_n = \Omega_n$ are given in units of $1/L_x$ ($k_n L_x$ is dimensionless) and consequently time is measured in units of L_x.

IV. PARTICLE CREATION

In this section, we shall show the particle creation for the different physical situations considered above. In all cases, we shall show that the numerical results obtained are in complete agreement with the analytical predictions existing in the literature.

A. Dirichlet and Neumann boundary conditions

When studying the particle creation in a cavity with moving walls, it is important to study the energy spectrum inside the cavity. For both Dirichlet (DBC) and Neumann boundary conditions (NBC), the eigenfrequencies inside the cavity satisfy the following condition:

$$\omega_n(t) = \frac{1}{L_x(t)}\sqrt{(\pi n)^2 + M^2}, \quad (17)$$

where n is natural number. If the field is massless (which corresponds to a one-dimensional cavity), then the spectrum is equidistant; i.e., the difference between two consecutive eigenfrequencies is constant. Otherwise, if M has nonzero values, the spectrum is nonequidistant, corresponding to the one of a three-dimensional cavity.

For example, by allowing the wall to have a frequency $\Omega = 2\omega_1$, we can see that the particle creation inside the cavity behaves as shown in Fig. 1(a). It has already been derived analytically that for a perturbation of the field mode equation, the particle creation is quadratic in time [holding for times $\sim 1/(\epsilon)$] and linear for a later time regime [32]. The numerical results perfectly agree with the analytical predictions at times $t \leqslant 1/\epsilon$ showing the initial quadratic increase of the total particle number and the number of particles created in the resonance mode $n = 1$. Some analytical approaches, as multiple scale analysis (MSA), reproduce these results if $\epsilon \ll 1$. However, by solving the equation of motion of each field mode [Eq. (A1)], we can go beyond the multiple scale analysis and see that the particle creation is exponential at very long times.

We can give further significance to the consideration of M in Eq. (17). If we assume that the mass parameter is $M = L_0 k_\parallel$, we can identify $k_\parallel = \pi\sqrt{(n_y/L_y)^2 + (n_z/L_z)^2}$ to nondynamical cavity dimensions. Then, the number of TE-mode photons created in a three-dimensional cavity equals the number of

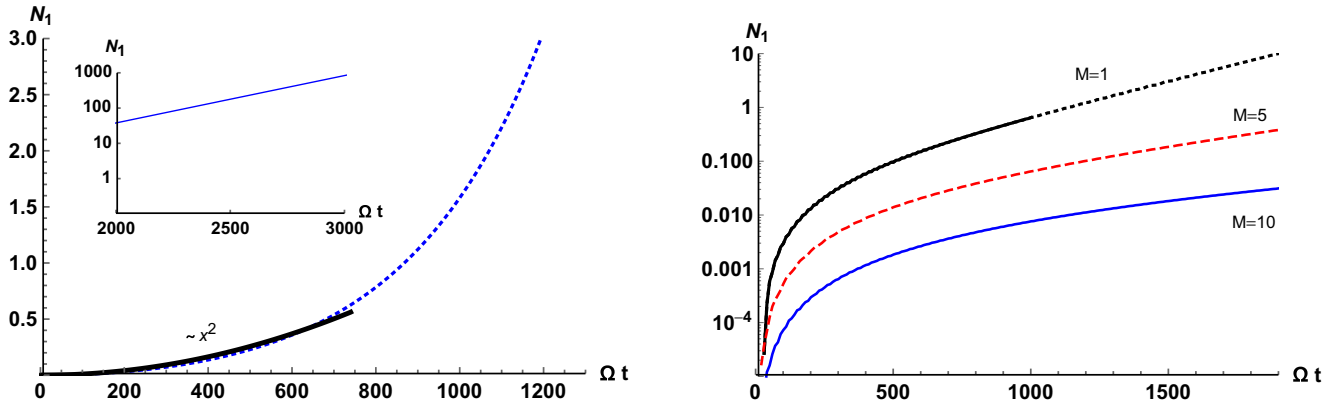

FIG. 1. (a) Left: Number of particles for the mode field 1, N_1, of a massless field inside a cavity with a moving wall under the perturbation $\Omega = 2\omega_1$ with DBC. Parameters used: $\epsilon = 0.001$, $\Lambda = \Lambda_m = 25$. (b) Right: LogPlot behavior for the number of particles created N_1 coefficient for different values of the mass parameter M under the perturbation of $\Omega = 2\omega_1$ under DBC, such as $M = 1$, $M = 5$, and $M = 10$. Parameters used: $\epsilon = 0.001$, $\Lambda = 10$, $\Lambda = 25$, and $\Lambda_m = 25$.

scalar particles of mass $k_\parallel$ created in a one-dimensional cavity [35]. If we consider that the field has mass, then we can see that the spectrum becomes nonequidistant and the particle creation behaves different as it is exponential at very short times. For a nonequidistant spectrum, in Fig. 1(b), we show the number of particles created for the mode 1 of the field and different values of the mass. This result has been obtained by an analytical approach [32,36], assuming a small perturbation leading to an exponential growth defined as $N_1(t) = \sinh(\pi^2\epsilon t/4L_0\sqrt{\pi^2 + M^2L_0^2})^2$ for the first mode [36]. This exponential behavior again agrees with our results; however, we do not have the constraint of a small perturbative motion as we solve the equation of motion of all field modes.

As said before, the only assumption we make is the number of field modes Λ that the field contains. We can investigate how fast we reach a stable solution as function of the number of modes used to solve the set of coupled differential equations [Eq. (A1)] in order to assure autonomy of the solution obtained. In Fig. 2(a), we show the total number of particles N_t created for a fixed time by changing the total number of modes for the parameters considered in Fig. 1(a). Since the DBC yields the simplest set of differential coupled equations, in this case, a total number of field modes of $\Lambda = 10$ already gives an accurate solution, being very reliable when $\Lambda \geqslant 20$. In Fig. 1(b), we plot the number of particles created N_1 for $M = 1$ for $\Lambda = 10$ (stronger dashed black line) and $\Lambda = 25$ thinner dotted black line. We can note that black dashes and black dots overlap, meaning that the precision of the solution is very accurate for both cases (considering $\Lambda = \Lambda_m$).

As the electromagnetic field involves both Neumann and Dirichlet boundary conditions, we can analyze separately a scalar field satisfying DBC and generalized NBC. This can be done this way since TE modes of the electromagnetic field are essentially described by Dirichlet scalar field, while TM modes correspond to a Neumann scalar field (as explained in Sec. II). In Fig. 2(b), we present the resonant photon creation inside a three-dimensional oscillating cavity taking the vector nature of the electromagnetic field into account. We compute the number of particles created N_1 for a massless field for both Dirichlet (blue dashes) and Neumann (red dots) conditions

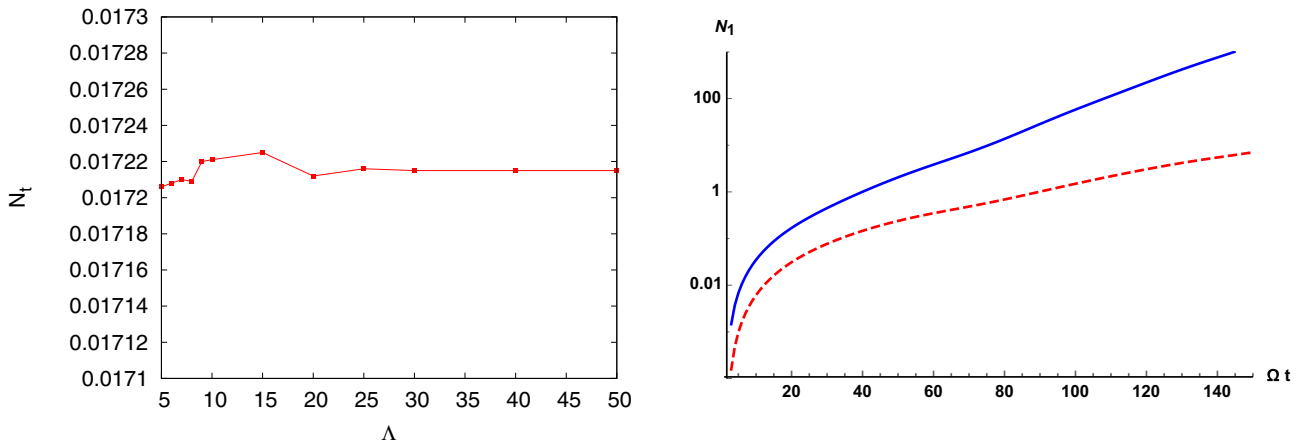

FIG. 2. (a) Left: Total number of particles created inside a cavity with DBC and zero mass as function of the total number of field modes Λ considered at a fixed time. Parameters used: $\epsilon = 0.01$, $\Omega = 2\omega_1$. (b) Right: Number of particles for the mode field 1, N_1, of a massless field inside a cavity with a moving wall under the perturbation $\Omega = 2\omega_1$ with DBC (red dashes) and generalized NBC (blue line). Parameters used: $\epsilon = 0.01$, $M = 0.5$.

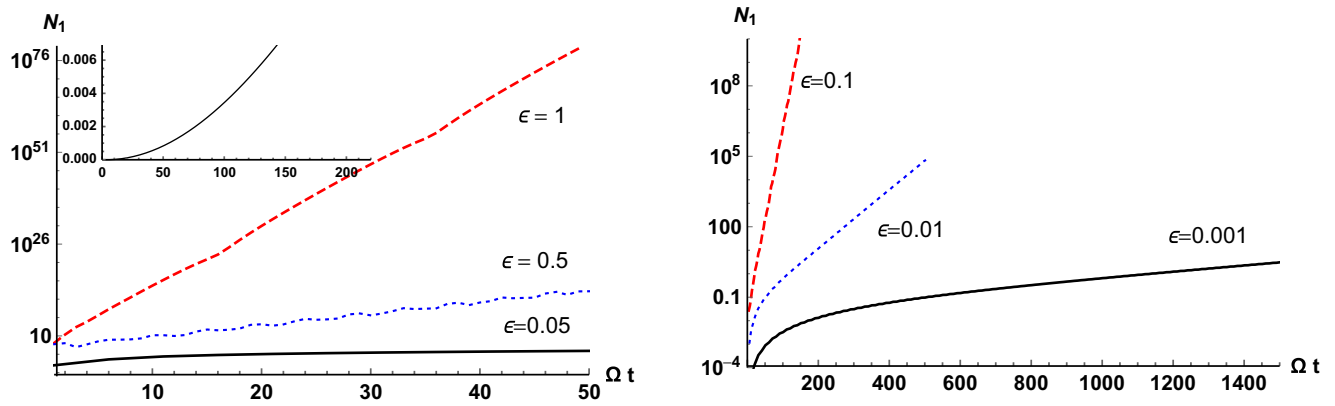

FIG. 3. Particle creation when the wall is excited as $\Omega = 2\omega_1$ for different fields in the cavity obeying DBC: (a) one-dimensional field ($M = 0$) and (b) a massive field $M = 1$. In all cases, we show different values of ϵ.

under resonance condition $\Omega = 2\omega_1$. In Ref. [32], authors have studied in detail the resonant situation $\Omega = 2\omega_k$, and showed that the exponential growth of created photons is greater for TM modes. This implies a novel contribution since there has been no numerical verification of this result.

B. Results beyond analytical estimations

In the following, we shall show results beyond analytical estimations. As we do not consider any approximation in our numerical approach, we can numerically estimate the behavior of particle creation when the motion of the cavity wall is considered arbitrary. It is important to note that the motion of the wall must be described by smooth and derivable functions in order to avoid the creation of spurious particle. In addition, the cavity wall has to return to its original position after a time T_F has elapsed. However, we are not limited to perturbative motions and can consider different values of ϵ, as can be observed in Figs. 3(a) and 3(b).

In Fig. 3(a), we show the particle creation for a scalar field satisfying DBC ($M = 0$). For this situation, it is well known that particles are created quadratically in the perturbative regime for times $t \leqslant 1/\epsilon$. However, for bigger values of ϵ, no analytical prediction has been obtained. As has been shown, we can obtain the expected results in the corresponding limits. In addition, we can predict that for bigger values of ϵ, the behavior is no longer a power law function. In Fig. 3(b), we show the particle creation for a massive field satisfying DBC. In this case, we choose $M = 1$ and compute the particle creation for different values of ϵ. It is easy to note the behavior predicted by Refs. [30,32,36] by the MSA analytical estimations for $\epsilon = 0.001$ in times $t \leqslant 1/\epsilon$. However, we can add information as for how the particle creation behaves as ϵ increases.

C. Generalized Robin boundary conditions

As for generalized Robin boundary conditions (RBC), the eigenfrequencies inside the cavity should satisfy a more difficult relation, such as [23,46]

$$(\omega_n L_x)\tan(\omega_n L_x) + \chi_0(\omega_n L_x)^2 = b_0\cos(f_0). \qquad (18)$$

We numerically solve this transcendent equation using a single Newton-Raphson method with an stopping error of 10^{-16}. We therefore obtain the eigenfrequencies inside the superconducting cavity as shown in Fig. 4, where we have plotted the difference of consecutive eigenfrequencies (from frequency ω_1 to frequency ω_6) for different parameters of the cavity. If we leave the experimental value $\chi_0 = 0.05$ fixed, we can study the difference between consecutive eigenfrequencies as a function of V_0. We can see that as the value of V_0 is bigger, the the spectrum is more equidistant.

In Fig. 4, we can note that there is an equidistant and a nonequidistant region of the cavity spectrum (different from the other case). This particularity allows us to interpolate between different situations. This means that by setting the parameters of the generalized RBC, we can reobtain results corresponding to either DBC and NBC (depending on which term is nonzero) [see Eq. (A8)], or in other case, explore new physical situations.

In Fig. 5(a), we present the number of particles created N_1 for a massless field in a superconducting waveguide satisfying generalized RBC by solving the set of differential equations presented in Eqs. (A6) and (A8). By choosing parameters $V_0 = 20$ and $\epsilon = 0.005$, we convert the generalized RBC into

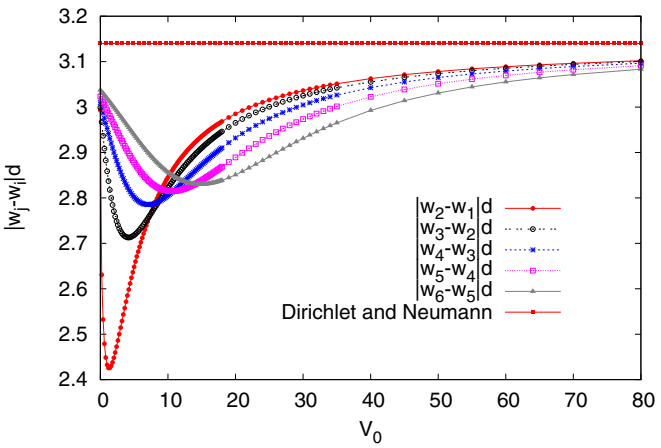

FIG. 4. Difference of consecutive eigenfrequencies as a function of $V_0 = b_0\cos(f_0)$, for a fixed value of $\chi_0 = 0.05$ for generalised Robin boundary conditions. The constant line represents the difference of consecutive frequencies for all values of cavity for Dirichlet and generalized Neumann conditions.

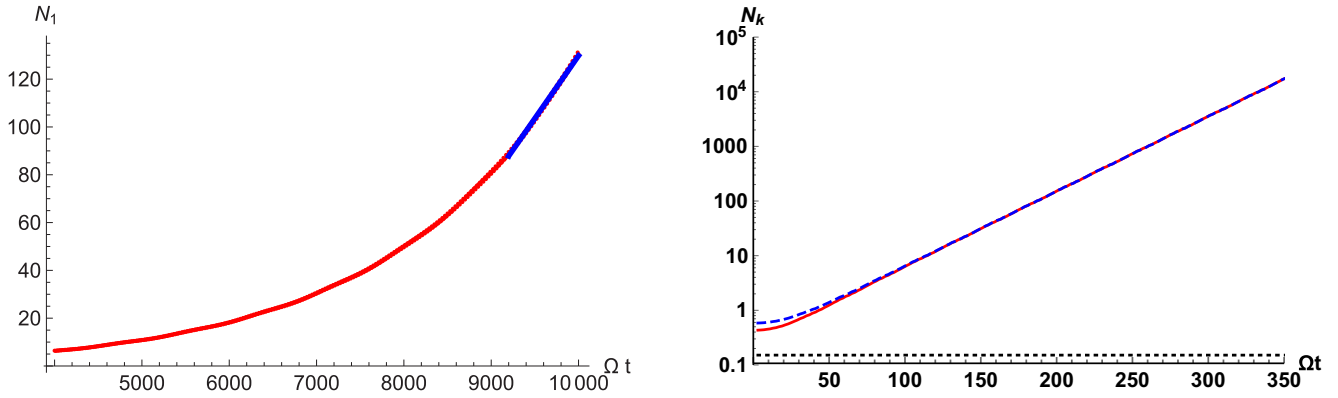

FIG. 5. (a) Left: Number of particles created N_1 under the perturbation of $\Omega = 2\omega_1$ for $V_0 = 20$, and a small perturbation amplitude $\epsilon = 0.005$, so as to have $V_0\epsilon \sim 0.1$. For equidistant spectra, the coupling between an infinite number of modes generates a quadratic and linear growth in the number of particles, for short and long timescales respectively. (b) Right: LogPlot behavior of the number of particles created N_k coefficient for a short temporal scale under a perturbation of $\Omega = 2\omega_1$ for $V_0 = 1$, $\chi_0 = 0.05$, and $\epsilon = 0.001$. We show the behavior of the number of particles created for the first eigenstate of eigenfrequency $\omega_1 = 0.8495$ (red and blue dashed lines) and for the second eigenstate of $\omega_2 = 3.2819$ (black dotted line). The difference between the red and blue dashed lines is that we consider different values of Λ_m. It is shown that N_k grows exponentially for N_1 as expected since the spectrum is nonequidistant. Parameters used: $\Lambda = 10$.

a DBC. This means that by setting the right combination of parameters, we are investigating the equidistant part of the spectrum. As expected, we verify that the coupling between infinite numbers of modes generates a quadratic or linear growth of the number of particles for short and long timescales respectively. In this case, it is possible to check that $V_0\epsilon \leqslant 1$ and then MSA still applies [25], yielding an exponential growth at longer times and showing results similar to the Dirichlet case. In fact, this is a case where we can reproduce Dirichlet results by considering a low-amplitude perturbation in the equations of generalized RBC [43]. In Fig. 5(a), for longer times, we draw a blue thick slope, which corresponds to the linear growth predicted by the MSA analytical approach, while the quadratic behavior of shorter times is generally predicted by a simpler perturbative approach.

In Fig. 5(b), we still consider a massless field satisfying generalized RBC. However, we choose parameters in the nonequidistant region of the spectrum, for example, by setting $V_0 = 1$, $\epsilon = 0.001$, and $\chi_0 = 0.05$. In that case, $\omega_1 = 0.8495$, $\omega_2 = 3.2819$, and $\omega_3 = 6.1403$, just to mention a few eigenfrequencies. By driving the cavity with an external frequency $\Omega = 2\omega_1$, we see the exponential growth in the number of particles created in mode field one N_1. It is important to note that $\Omega \neq |\omega_i \pm \omega_j|$, which means there is only one single mode under parametric resonance. As one expects, if the only resonant mode is tuned with the external frequency Ω, the number of created particles in this mode grows exponentially [similarly to Fig. 1(b) with different boundary conditions]. In this case, we have solved the problem by using different values of Λ_m. In the red solid line of Fig. 5(b) we have used $\Lambda_m = 10$ and in the blue dashed line $\Lambda_m = 30$. We have verified that for values $\Lambda_m \geqslant 30$ the results obtained are similar. The difference between both curves is only noticeable at short times. The black line corresponds to the second eigenfrequency, which

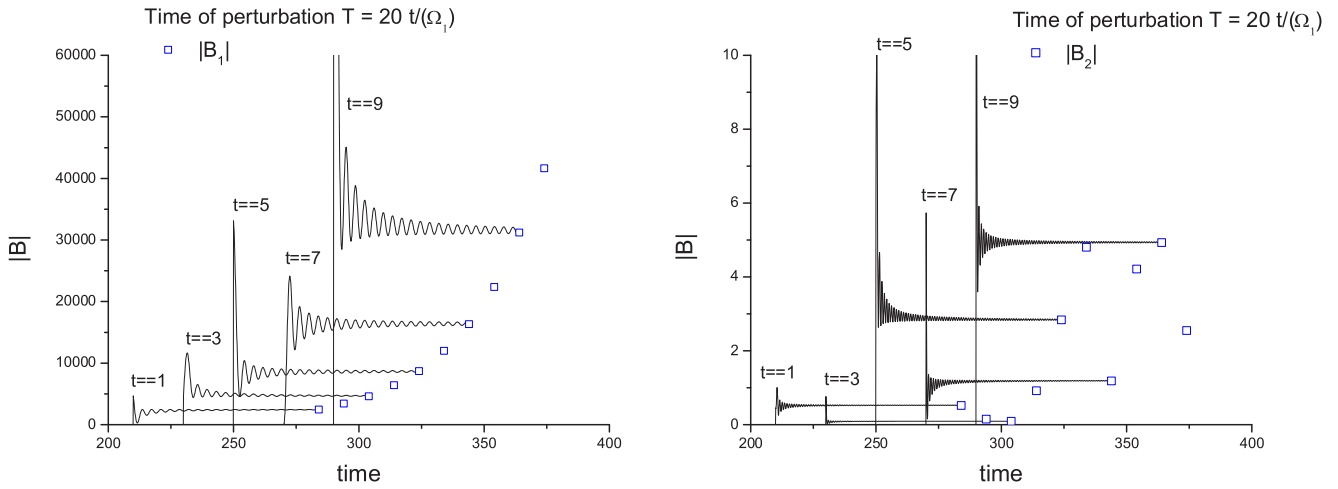

FIG. 6. (a) Absolute value of B_1 as function of time to show the role of the time t_F for which the perturbation is on. It can be seen that the number of particles $\mathcal{N}_1 = |B_1|^2/(2\omega_1)$ is increased as the perturbation time is longer. Parameters used: $\Omega = 2\omega_1$, or $V_0 = 1$, $\xi = 0.05$, and $\epsilon = 0.001$. (b) Absolute value of B_2 as function of time to show the role of the time t_F, which is considerably smaller compared with B_1 for the same time.

is not excited. The freedom for choosing different parameters in order to transform RBC into already known situations (as DBC) allows us to cross-check analytical results and makes our numerical scheme reliable.

In order to set some light into the numerical scheme, in Fig. 6, we show the absolute value of the coefficient B, which is numerically related to the number of particles created $N_k = |B_k|^2/(2\omega_k)$, where k is the field mode considered. Therein, we show how the value of this coefficient grows in time, as the perturbation time is turned on for longer times. In Fig. 6(a), we show the behavior of $|B_1|$ for the same parameters used in Fig. 1(b), while in Fig. 6(b), we present $|B_2|$. It is clear to see that the leading term is the one related to the field mode 1. This schematic representation applies to all cases considered.

V. CONCLUSIONS

We present an alternative numerical approach to simulate the process of photon generation in a cavity in which one mirror is forced to oscillate in a prescribed way. The focus is not restricted to one-dimensional models, but three-dimensional (3D) cavities are studied as well, beyond the perturbative regime, which is shown to be recovered in the appropriate limit. We are also not restricted on the type of boundary condition used. In our numerical approach, we can choose to use Dirichlet, Neumann, or generalized Robin conditions, allowing the computation of particle creation in time regimes beyond any analytical prediction. In our approach, we take advantage of the analytical studies obtained in the area and present a global numerical approach. Our numerical scheme is based on the resolution of the equations of field modes with different time-dependent boundary conditions (without constraints in the wall motion) and a further comparison between the ground state before and after the movement of the cavity wall. We selectively focus on obtaining the information required for the calculation of the number of particles created, relying only on numerical schemes.

We have considered a cavity with a moving wall at one end $x = L_x(t)$, while the other wall at $x = 0$ remains at rest. We have derived the set of differential equations for the canonical variables in each case considered and computed numerically the number of particles created. For example, by considering separately the Dirichlet and Neumann cases, we have solved the TE and TM modes of the electromagnetic field inside the cavity, reproducing previous analytical predictions. We have also shown that by considering Neumann (at $x = 0$) and generalized Robin boundary conditions (at $x = L_x$), we simulate a waveguide superconducting cavity terminated with a SQUID at one end, which is the promising experimental setup for measuring the DCE. We have further shown that by introducing the parameter M, we can reproduce the creation of particles for a 3D cavity, while if $M = 0$, then the scalar field is inside a 1D cavity. In all cases, we have shown that the rate of particle production depends strongly on whether the frequency spectrum is equidistant or not.

In all cases considered, we have presented the number of particles created. We have, for example, reobtained already known results in the simplest cases of 1D massive and massless field with Dirichlet boundary conditions. These examples validate our numerical scheme. We have further presented results that have been longer predicted but never demonstrated as the bigger rate of TM photons compared to TE photons. In the case of generalized Robin boundary conditions, we have obtained expected results for an equidistant spectrum and for a nonequidistant one. Hence, the formalism presented in this paper can be used to cross-check analytical results also in this realistic case, which might be of importance for future experiments. Finally, we have also shown excellent agreement of our numerical scheme with the theoretical predictions and with other numerical approaches.

With our formalism at hand, the DCE can be investigated fully numerically, making it possible to study a variety of scenarios where no analytical results are known, such as large-amplitude oscillations and arbitrary wall motions. By considering this numerical approach, we gain confidence in our numerical method by reproducing already known analytical results. This allows us to explore, on the one hand, regions of the frequency spectrum that cannot be yet reached because of analytical difficulties in the development of solutions, and on the other, multimode couplings beyond MSA (i.e., longer times). This approach can be easily extended to having two moving mirrors by adding a time-dependent boundary conditions to the $x = 0$ extreme [47]. Finally, it is worth mentioning that this method can be used to study the generation of squeezed states of light in moving cavities, as studied in Ref. [48].

ACKNOWLEDGMENT

This work was supported by ANPCyT (Argentina), CONICET (Argentina) and UBA (Argentina).

APPENDIX A: BOUNDARY CONDITIONS CONSIDERED

In this appendix, we present the set of differential coupled equations for the canonical variables Q_k^n determined by the use of different boundary conditions when considering Eq. (6) in Sec. II.

1. Dirichlet boundary condition (DBC)

We first present the set of coupled differential equations for the canonical variables obtained when the field inside the cavity satisfies DBC, expressed by

$$\begin{aligned}\dot{Q}_m &= U_m,\\ \dot{U}_m &= -\omega_m^2(t)Q_m + 2\lambda(t)\sum_s S^D_{ms}\dot{Q}_s + \dot{\lambda}(t)\sum_s S^D_{ms}Q_s\\ &\quad + \lambda^2(t)\sum_{l,s} S^D_{lm}S^D_{ls}Q_s,\end{aligned} \tag{A1}$$

where S^D_{ms} is a coupling matrix, and takes the form

$$S^D_{ms} = \begin{cases} 0 & \text{if } m = s\\ (-1)^{s+m}\frac{2ms}{(m^2-s^2)} & \text{otherwise}\end{cases} \tag{A2}$$

and $\lambda(t) = \frac{\dot{L}_x(t)}{L_x(t)}$.

2. Neumann boundary condition (NBC)

In the case when the field inside the cavity satisfies NBC, the procedure is similar, but the coupling matrices S_{ms}, T_{ms}, and V_{ms} are more complicated, defined in this case as

$$\begin{aligned}\dot{Q}_m &= U_m,\\ \dot{U}_m &= -\omega_m^2(t)Q_m - 2\lambda(t)\sum_s S^N_{ms}\dot{Q}_s - \dot{\lambda}(t)\sum_s S^N_{ms}Q_s - 2L_x^2(t)\dot{\lambda}(t)\sum_s T_{ms}\ddot{Q}_s\\ &\quad - \sum_s \left(L_x^2\ddot{\lambda}T_{ms} - \lambda(t)R_{ms}(t,\dots)\right)\dot{Q}_s - L_x^2\lambda(t)\sum_s T_{ms}\dddot{Q}_s,\end{aligned}$$

where the coupling matrices are

$$S^N_{ms} = \begin{cases} -1 & \text{if } m = s\\ (-1)^{s+m}\frac{2ms}{(m^2-s^2)} & \text{if } m \neq s\end{cases}, \tag{A3}$$

$$T_{ms} = \begin{cases} \frac{1}{15} - \frac{-3+(\pi m)^2}{4(\pi m)^4} & \text{if } m = s\\ \frac{(m-s)^4\{-12+[\pi(m+s)]^2\}\cos[\pi(m+s)]}{[(m^2-s^2)\pi]^4} - (m+s)^4\{-12+[\pi(m-s)]^2\}\cos[\pi(m-s)] & \text{if } m \neq s\end{cases} \tag{A4}$$

$$R_{ms} = \begin{cases} -\frac{8(m\pi)^8(33+2L_0^2)+315[-34(m\pi)^6+8(m\pi)^8-315L_0^2+3(m\pi)^4(46-5L_0^2)+15(m\pi)^2(-18+11L_0^2)\cos(2m\pi)]}{2520(m\pi)^8} & \text{if } m = s\\ \frac{1}{\pi^8}\frac{\{10080L_0^2-(m-s)^2\pi^2(-2160+1320L_0^2+(m-s)^2\pi^2\{276+\pi^2[-29m^2+34ms-5s^2+2m(m-s)^3\pi^2]-30L_0^2\})\}\cos[\pi(m-s)]}{(m-s)^8} & \\ +\frac{[10080L_0^2-(m+s)^2\pi^2(-2160+1320L_0^2+(m+s)^2\pi^2\{276+(m+s)\pi^2[-29m-5s+2m(m+s)^2\pi^2]-30L_0^2\})]\cos[\pi(m+s)]}{(m+s)^8}) & \text{if } m \neq s.\end{cases} \tag{A5}$$

3. Robin boundary condition (RBC)

A promising setup in order to experimentally study the DCE consists of a superconducting waveguide ended with a SQUID that determines the boundary condition of the field at that point [23]. A time-dependent magnetic flux through the SQUID generates a time-dependent boundary condition, with the subsequent excitation of the field (particle creation) in the waveguide. The electromagnetic field inside the cavity can be described by a single quantum massless scalar field satisfying NBC in $x = 0$ and generalized RBC in $x = L_x$ (assuming a SQUID located at L_x). From a mathematical point of view, the system is therefore modeled by a massless scalar field satisfying generalized RBC. The set of equations for the canonical variables related to the field modes are

$$\begin{aligned}\dot{Q}_m &= U_m,\\ \dot{U}_m &= \omega_m^2(t)Q_m + \sum_s S^R_{ms}Q_s,\end{aligned} \tag{A6}$$

with

$$S^R_{ms} = \frac{2\epsilon b_0}{\sqrt{M_m M_s}}\sin(f_0)\sin(\Omega t)\cos(\omega_m L_x)\cos(\omega_s L_x). \tag{A7}$$

and $M_m = 1 + \frac{\sin(2\omega_m L_x)}{2\omega_m L_x} + \frac{\chi_0}{L_x}\cos(\omega_m L_x)^2$ with b_0 and χ_0 dimensionless physical quantities. $f(t)$ is the phase across the SQUID controlled by an external magnetic flux and defined as $\cos[f(t)] = \cos[f_0 + \epsilon\cos(\Omega t)]$ [43], obtaining a boundary condition described as

$$\chi_0\ddot{\phi}_{L_x} + b_0\cos[f(t)]\phi_{L_x} + \phi'_{L_x} = 0, \tag{A8}$$

with $b_0 = 2E_j/E_{L_{cav}}$ and $\chi_0 = 2C_j/(C_0L_x)$, all physical parameters defined in [23].

APPENDIX B: COMPARISON AMONG PREVIOUS NUMERICAL RESULTS

In Refs. [30,36], the authors show that the number of TE-mode photons created in a three-dimensional cavity equals the number of scalar particles of mass $k_\perp$ created in a one-dimensional cavity of length $[0, L_x(t)]$. Considering a periodic trajectory of the moving mirror

$$L_x(t) = L_x[1 - \epsilon\sin(\Omega t)], \quad \epsilon \ll 1,$$

In a resonantly vibrating cavity $\Omega = 2\omega_n$, the number of TE-mode photons created in the resonant mode increases exponentially in time as

$$N_n(t) = \sinh^2(n\gamma_n\epsilon t), \quad \text{with} \quad \gamma_n = \frac{n}{4\omega_n}\left(\frac{\pi}{L_x}\right)^2, \tag{B1}$$

with ω_n defined as in Eq. (17) and L_x being the initial length of the one-dimensional cavity.

In the present paper, we propose a fully numerical approach following the analytical expressions for the mode field equations developed in Refs. [30,32]. The only numerical approach existing in the literature corresponds to Refs. [35,36], which presented a formalism allowing numerical investigation of the DCE for scalar particles in one-dimensional cavity. In Ref. [35], the author studied the number of TE-mode photons created for a massless electromagnetic field, while in Ref. [36] the generalization of the method to higher dimension has been presented. As explained in the main text, the number of particles created is defined by the comparison between the ground state before and after the movement of the cavity wall, explicitly defined as in Eq. (15). The author then introduces auxiliary functions ξ_n^m and η_n^m to explicitly find the expression for the Bogoliubov coeficients α_{mn} and β_{mn}. Through these

auxiliary functions, the author is making a transformation into a known basis, ensuring the new variables satisfied the equation of motion and the same boundary conditions (Dirichlet). In Ref. [36], these coefficients are presented:

$$\alpha_{mn}(t_F) = \frac{1}{2}\sqrt{\frac{\Omega_n^F}{\Omega_n^0}}\left[\Delta_n^+(t_F)\xi_n^m(t_F) + \Delta_n^-(t_F)\eta_n^m(t_F)\right], \quad \text{(B2)}$$

$$\beta_{mn}(t_F) = \frac{1}{2}\sqrt{\frac{\Omega_n^F}{\Omega_n^0}}\left[\Delta_n^-(t_F)\xi_n^m(t_F) + \Delta_n^+(t_F)\eta_n^m(t_F)\right], \quad \text{(B3)}$$

with $\Delta_n^{\pm}(t) = 1/2[1 \pm \Omega_n^0/\Omega_n(t)]$ as defined in Ref. [36]. In this way, Ref. [36] has complete knowledge of the final state and can compute the number of created particles by means of Eqs. (B3) and (15). After obtaining this analytical result, a numerical implementation is applied based on these expressions. The numerical results presented were entirely in very good agreement with the corresponding analytical predictions derived for small amplitude oscillations $\epsilon \ll 1$, which demonstrates the reliability of the numerical simulations. However, the highest drawback of the approach presented in Refs. [35,36] is that more complicated boundary conditions appearing, for example, when studying TM-mode photons cannot be treated within that approach. This is because they cannot obtain the corresponding expression for α_{mn} and β_{mn} in the case of more complicated boundary conditions.

In contrast, with our numerical approach we do not focus on the exact expressions for α_{mn} and β_{mn}. We proceed alternately to compute the number of particles created. We assume that the unperturbed solution has the form of:

$$Q_n(t \geqslant t_F) = \frac{1}{\sqrt{2\omega_n^F}}\left[\hat{A}_n(t_F)e^{-i\omega_n^F t} + \hat{B}_n(t_F)e^{i\omega_n^F t}\right], \quad \text{(B4)}$$

with ω_n^F being the frequency for $t \geqslant t_F$ as explained in the main text. We therefore can multiply both terms of the equation by $\exp(-i\omega_n^1 t)$ and take the mean value in $t_F < t < t_{\max}$. In this way, we are able to numerically evaluate $|B_n|^2$ and also the particle number in field mode n as a function of time as $N_n(t) = |B_n(t)|^2/(2\omega_n^F)$. In our numerical approach, we solve the equation of motion for the field modes (for Dirichlet, generalized Neumann, and generalized Robin boundary conditions) and evaluate the number of particles created in each case.

In order to compare our numerical scheme with others reported in the literature, we consider Dirichlet boundary conditions. In the case of a three-dimensional cavity, we can reproduce the analytical result derived in Ref. [32] and compare with the results obtained by the numerical approach proposed in Ref. [35] (also programmed by us).

In Fig. 7, we show the numerical results obtained by our approach in the case of a three-dimensional cavity with Dirichlet boundary conditions and compare them with the analytical prediction [32] and previous results in the literature. As we can see, our result agrees very accurately with the analytical prediction up to times of order $1/\epsilon$ by considering only ten field modes involved, i.e., a frequency cutoff of $\Lambda = 10$. Our method can be improved by considering a bigger number of modes involved. Within our formalism, the DCE can be investigated fully numerically, making it possible to study

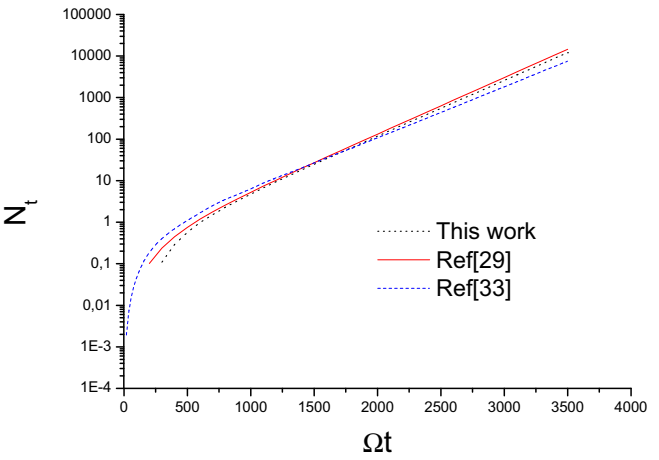

FIG. 7. We show the analytical prediction of Ref. [32] for the number of TE-mode photons created in mode n with a solid red line. With a blue dashed line, we present the curve predicted by the numerical approach of Ruser and with a black dotted line, we show our numerical results. Parameters used: $\epsilon = 0.001$, $M = 0.2$, $L_x = 1.0$, $\Lambda = 10$, and $n = 1$.

a variety of scenarios where no analytical results are known (large-amplitude oscillations and arbitrary wall motions etc). Our main advantage is that we can apply this formalism to more general boundary conditions such as generalized NBC and RBC (contrary to Refs. [35,36]).

APPENDIX C: CODE DESCRIPTION AND COMPUTATIONAL PERFORMANCE

The code was written in FORTRAN 90 and was running on several computers with processor I7 3.6 and Intel Xeon 2.4. Distributed parallelism was implemented using the OPENMP standard. The integration in time of the modes following the Runge-Kutta fourth-order method with accelerator of Mayer is the most demanding part of the code, consuming 95% of the calculations. Incrementing the number of coupled modes

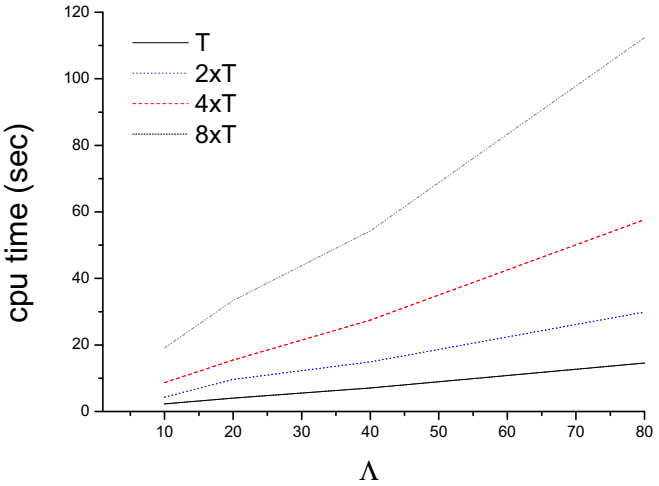

FIG. 8. Time consumed in calculations as a function of the number of modes Λ considered in the electromagnetic field.

having geometric intensification of the time consumed that is the reason why it was important to establish the minimal number of modes for which the results were accurate enough in the first place. We have noted that a cutoff of $\Lambda \sim 17$ was a good number of field modes involved to obtain accurate simulations and reproduce analytical results [as shown in Fig. 2(a)]. Consider that we need to solve a $[4 \times \Lambda]$ set of coupled differential equations of first order in each time step. [See Eq. (7), real and imaginary parts.]

In Fig. 8 we plot for a general case the time consumed in calculations for obtaining 10 points of the curve $|B^2|$ in function of time (see Fig. 6 for a description of numerical scheme). We increase the number of modes used (in the x axis), increasing the final time t_F at which the wall remains at rest again, for four different values of T ($T = 100$ numerical time units). In this way, we compute $|B^2|$. It is easy to note that the time consumed depends strongly of the number of modes, especially for large times.

[1] J. Schwinger, Proc. Natl. Acad. Sci. USA **90**, 958 (1993); **90**, 2105 (1993); **90**, 4505 (1993); **90**, 7285 (1993).
[2] V. V. Dodonov, Phys. Scr. **82**, 038105 (2010).
[3] D. A. R. Dalvit, P. A. Maia Neto, and F. D. Mazzitelli, Lect. Notes Phys. **834**, 419 (2011).
[4] P. D. Nation, J. R. Johansson, M. P. Blencowe, and F. Nori, Rev. Mod. Phys. **84**, 1 (2012).
[5] V. V. Dodonov, Adv. Chem. Phys. **119**, 309 (2001).
[6] A. Lambrecht, M.-T. Jaekel, and S. Reynaud, Phys. Rev. Lett. **77**, 615 (1996).
[7] G. T. Moore, J. Mater. Phys. **11**, 2679 (1970).
[8] S. A. Fulling and P. C. W. Davies, Proc. R. Soc. London, Ser. A **348**, 393 (1976).
[9] B. Dewitt, Phys. Rep. **19**, 295 (1975).
[10] C. M. Wilson, G. Johansson, A. Pourkabirian, J. R. Johansson, T. Duty, F. Nori, and P. Delsing, Nature (London) **479**, 376 (2011).
[11] P. Lahteenmaki, G. S. Paraoanu, J. Hassel, and P. J. Hakonen, Proc. Natl. Acad. Sci. USA **110**, 4234 (2013).
[12] S. Felicetti, C. Sabín, I. Fuentes, L. Lamata, G. Romero, and E. Solano, Phys. Rev. B **92**, 064501 (2015).
[13] G. Benenti, A. D'Arrigo, S. Siccardi, and G. Strini, Phys. Rev. A **90**, 052313 (2014).
[14] J. R. Johansson, G. Johansson, C. M. Wilson, P. Delsing, and F. Nori, Phys. Rev. A **87**, 043804 (2013).
[15] S. Felicetti, M. Sanz, L. Lamata, G. Romero, G. Johansson, P. Delsing, and E. Solano, Phys. Rev. Lett. **113**, 093602 (2014).
[16] R. Stassi, S. De Liberato, L. Garziano, B. Spagnolo, and S. Savasta, Phys. Rev. A **92**, 013830 (2015).
[17] A. Agnesi, C. Braggio, G. Bressi, G. Carugno, G. Galeazzi, F. Pirzio, G. Reali, G. Ruoso, and D. Zanello, J. Phys. A: Math. Theor. **41**, 164024 (2008). For a model with time-dependent conductivity, see M. Crocce, D. A. R. Dalvit, F. C. Lombardo, and F. D. Mazzitelli, Phys. Rev. A **70**, 033811 (2004).
[18] W.-J. Kim, J. H. Brownell, and R. Onofrio, Phys. Rev. Lett. **96**, 200402 (2006).
[19] J. Doukas and J. Louko, Phys. Rev. D **91**, 044010 (2015).
[20] B. Mintz, C. Farina, P. A. Maia Neto, and R. B. Rodrigues, J. Phys. A **39**, 11325 (2006).
[21] J. R. Johansson, G. Johansson, C. M. Wilson, and F. Nori, Phys. Rev. A **82**, 052509 (2010).
[22] A. L. C. Rego, H. O. Silva, D. T. Alves, and C. Farina, Phys. Rev. D **90**, 025003 (2014).
[23] W. Wustmann and V. Shumeiko, Phys. Rev. B **87**, 184501 (2013).
[24] V. V. Dodonov, A. B. Klimov, and D. E. Nikonov, J. Math. Phys. **34**, 2742 (1993).
[25] V. V. Dodonov and A. B. Klimov, Phys. Rev. A **53**, 2664 (1996).
[26] V. V. Dodonov, Phys. Lett. A **244**, 517 (1998).
[27] A. V. Dodonov and V. V. Dodonov, Phys. Lett. A **289**, 291 (2001).
[28] J.-Y. Ji, H.-H. Jung, J.-W. Park, and K.-S. Soh, Phys. Rev. A **56**, 4440 (1997).
[29] A. B. Klimov and V. Altuzar, Phys. Lett. A **226**, 41 (1997).
[30] M. Crocce, D. A. R. Dalvit, and F. D. Mazzitelli, Phys. Rev. A **64**, 013808 (2001).
[31] D. F. Mundarain and P. A. M. Neto, Phys. Rev. A **57**, 1379 (1998).
[32] M. Crocce, D. A. R. Dalvit, and F. D. Mazzitelli, Phys. Rev. A **66**, 033811 (2002).
[33] V. V. Dodonov, Phys. Lett. A **207**, 126 (1995).
[34] A. V. Dodonov, E. V. Dodonov, and V. V. Dodonov, Phys. Lett. A **317**, 378 (2003).
[35] M. Ruser, J. Phys. A **39**, 6711 (2006).
[36] M. Ruser, Phys. Rev. A **73**, 043811 (2006).
[37] D. T. Alves and E. R. Granhen, Comput. Phys. Commun. **185**, 2101 (2014).
[38] D. T. Alves, E. R. Granhen, H. O. Silva, and M. G. Lima, Phys. Rev. D **81**, 025016 (2010).
[39] D. T. Alves, E. R. Granhen, and W. P. Pires, Phys. Rev. D **82**, 045028 (2010).
[40] D. T. Alves, E. R. Granhen, H. O. Silva, and M. G. Lima, Phys. Lett. A **374**, 3899 (2010).
[41] C. K. Cole and W. C. Schieve, Phys. Rev A **52**, 4405 (1995).
[42] C. K. Cole and W. C. Schieve, Phys. Rev A **64**, 023813 (2001).
[43] F. C. Lombardo, F. D. Mazzitelli, A. Soba, and P. I. Villar, Phys. Rev. A **93**, 032501 (2016).
[44] H. O. Silva and C. Farina, Phys. Rev D **84**, 045003 (2011); C. Farina, H. O. Silva, A. L. C. Rego, and D. T. Alves, Int. J. Mod. Phys. Conf. Ser. **14**, 306 (2012); A. L. C. Rego, B. W. Mintz, C. Farina, and D. T. Alves, Phys. Rev D **87**, 045024 (2013); A. L. C. Rego, J. P. da S. Alves, D. T. Alves, and C. Farina, Phys. Rev A **88**, 032515 (2013); J. D. L. Silva, A. N. Braga, A. L. C. Rego, and D. T. Alves, Phys. Rev. D **92**, 025040 (2015).
[45] L. F. Shampine, J. Sci. Comput. **25**, 3 (2005).
[46] C. D. Fosco, F. C. Lombardo, and F. D. Mazzitelli, Phys. Rev. D **87**, 105008 (2013).
[47] P. I. Villar, A. Soba, and F. C. Lombardo, Phys. Rev. A **95**, 032115 (2017).
[48] V. V. Dodonov, A. B. Klimov, and V. I. Manko, Phys. Lett. A **149**, 225 (1990).